Formation of Chlorinated Organic Compounds from Cl Atom-Initiated Reactions of Aromatics and Their Detection in Suburban Shanghai

Chuang Li[1], Lei Yao[1,2]*, Yuwei Wang[1], Mingliang Fang[1], Xiaojia Chen[1], Lihong Wang[1], Yueyang Li[1], Gan Yang[1], Lin Wang [1,2,3,4,5]*

[1] Shanghai Key Laboratory of Atmospheric Particle Pollution and Prevention (LAP[3]), Department of Environmental Science and Engineering, Jiangwan Campus, Fudan University, Shanghai 200438, China

[2] Shanghai Institute of Pollution Control and Ecological Security, Shanghai 200092, China

[3] IRDR International Center of Excellence on Risk Interconnectivity and Governance on Weather/Climate Extremes Impact and Public Health, Fudan University, Shanghai 200438, China

[4] National Observations and Research Station for Wetland Ecosystems of the Yangtze Estuary, Shanghai, 200433, China

[5] Collaborative Innovation Center of Climate Change, Nanjing, 210023, China

Corresponding Author: L.Y., email, lei_yao@fudan.edu.cn; phone, +86-21-31243568

L.W., email, lin_wang@fudan.edu.cn; phone, +86-21-31243568

Abstract. Chlorine (Cl) atoms generated from the photolysis of atmospheric reactive chlorine species can rapidly react with various volatile organic compounds (VOCs), forming chlorine- and non-chlorine-containing low-volatile oxygenated organic molecules. Yet, the formation mechanisms of chlorine-containing oxygenated organic molecules (Cl-OOMs) from reactions of Cl atoms with aromatics in the presence and absence of NO_x are not fully understood. Here, we investigated Cl-OOMs formation from Cl-initiated reactions of three typical aromatics (i.e., toluene, m-xylene, and 1,2,4-trimethylbenzene (1,2,4-TMB)) in the laboratory and searched for ambient gaseous Cl-OOMs in suburban Shanghai. From our laboratory experiments, 19 Cl-containing peroxyl radicals and a series of Cl-OOMs originating from the Cl-addition-initiated reaction were detected, which provides direct evidence that the Cl-addition-initiated reaction is a non-negligible pathway. In addition, a total of 51 gaseous Cl-OOMs were identified during the winter in suburban Shanghai, 38 of which were also observed in laboratory experiments, hinting that Cl-initiated reaction of aromatics could serve as a source of Cl-OOMs in an anthropogenically influenced atmosphere. Toxicity evaluation of these Cl-

33 OOMs shows potential adverse health effects. These findings demonstrate that Cl-OOMs can

34 be efficiently formed via the Cl-addition pathway in the reactions between aromatics and Cl

35 atoms and some of these Cl-OOMs could be toxic.

36
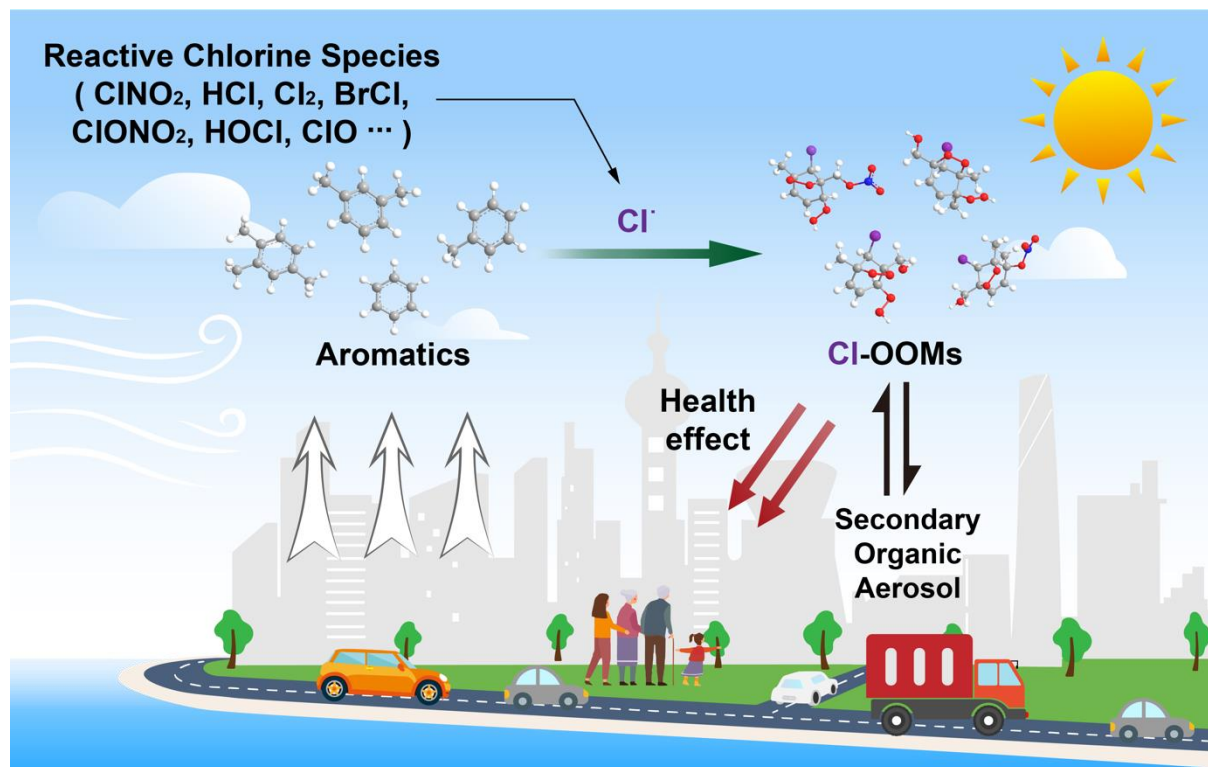
1. Introduction

Atmospheric chlorine atoms (Cl), together with hydroxyl radicals (OH), ozone (O_3), and nitrate radicals (NO_3), play vital roles in transforming volatile organic compounds (VOCs), leading to the formation of oxygenated organic molecules (OOMs) and secondary organic aerosol (SOA)(Priestley et al., 2018; Shang et al., 2021; Tham et al., 2016; Thornton et al., 2010). The involvement of Cl atoms in atmospheric chemical processes was conventionally thought to be confined to the oceanic boundary layer (Keene et al., 1999; Knipping et al., 2000). Estimated Cl atom concentrations in the coastal region ranged from 10^2 to 10^5 molecules cm^{-3} (Thornton et al., 2010; Wingenter et al., 2005). Recently, a number of reactive chlorine species, such as nitryl chloride ($ClNO_2$), chlorine nitrate ($ClONO_2$), hypochlorous (HOCl), chlorine (Cl_2), bromine chloride (BrCl), and hydrochloric acid (HCl), were found to lead to high concentrations of Cl atoms in the urban and suburban atmospheres (Breton et al., 2018; Peng et al., 2020; Priestley et al., 2018). During the daytime, peak Cl atom concentrations can reach 10^6 molecules cm^{-3} (Wang et al., 2023). which is still less than the global average concentrations of OH radicals (Breton et al., 2018; Liu et al., 2017). Nonetheless, the reaction rate coefficients of VOCs with Cl atoms are generally 1-2 orders of magnitude larger than those of OH radicals, which can partially compensate for the lower concentration of Cl atoms when determining the relative importance of different reactive loss pathways of VOCs (Chen et al., 2023; Riva et al., 2015; Wang et al., 2005).

Apart from H-abstraction, Cl atoms can be added to VOCs forming chlorine-containing oxygenated organic molecules (Cl-OOMs) in reactions of VOCs with Cl atoms. For small alkenes (e.g., isoprene), the reaction mechanism is dominated by Cl-addition to the double bond, with some allylic hydrogen abstraction (approximately 15% for isoprene at 1 atm) (Finlayson-Pitts et al., 1999; Orlando et al., 2003; Ragains and Finlayson-Pitts, 1997). For larger biogenic VOCs (e.g., β-pinene), which contain a greater number of abstractable hydrogen atoms, H-abstraction becomes more significant; for instance, H-abstraction is thought to account for half of the overall initiation reactions (Finlayson-Pitts et al., 1999). Overall, both Cl-addition and H-abstraction pathways coexist for biogenic VOCs, with the Cl-addition pathway possibly

65 being the more dominant pathway, such as isoprene (Wang et al., 2022) and d-limonene (Wang

66 et al., 2019).

67   Given the ubiquitous existence of aromatics in the urban air and the recent detection of

68 reactive chlorine species that are precursors of Cl atoms in the same atmosphere, the reaction

69 mechanisms of aromatics and Cl atoms should be of concern. Although the reaction rate

70 coefficient of benzene with Cl atoms under normal atmospheric conditions is relatively slow

71 $(1.3 \times 10^{-15}$ cm^3 molecule^{-1} s^{-1}) and this reaction is insignificant in the ambient atmosphere, its

72 reaction mechanism provides valuable insights into reaction pathways of Cl atoms and

73 aromatics (Shi and Bernhard, 1997). Sokolov *et al.* proposed that C_6H_6Cl radicals, formed

74 through a Cl-addition pathway in reactions of Cl atoms and benzene, can either decompose

75 back to benzene or further react in a non-aromatizing manner (Sokolov et al., 1998). In contrast,

76 toluene, xylene, and trimethylbenzene react with Cl atoms at faster rates, urging a better

77 understanding of their reaction mechanisms. Using the density functional theory and the

78 conventional transition state theory, Huang *et al.* investigated the Cl-toluene reaction (Huang

79 et al., 2012). Their findings indicate that the reaction rate coefficient for the H-abstraction

80 pathway $(5.58 \times 10^{-11}$ cm^3 molecule^{-1} s^{-1}) is substantially higher than that for the Cl- addition

81 pathway $(0.91 \times 10^{-11}$ cm^3 molecule^{-1} s^{-1}), highlighting the significance of the H-abstraction

82 pathway that accounts for approximately 86% of Cl-initiated reactions. Studies employing gas

83 chromatography-mass spectrometry (GC-MS) to examine products of Cl-initiated reactions of

84 toluene and iodide-based chemical ionization mass spectrometry (I-CIMS) to analyze products

85 of Cl-initiated reactions of m-xylene, have both predominantly detected chlorine-free

86 oxygenated organic compounds, which were supposed as main products (Cai et al., 2008; Wang

87 et al., 2005). These results have guided atmospheric models to integrate the H-abstraction as

88 the primary reaction pathway in their analytical frameworks (Ma et al., 2023; Peng et al., 2022).

89 However, studies focusing on the Cl-addition pathway and its related products are sparse, and

90 the significance of the Cl-addition pathway in the atmospheric reactions of Cl atoms and

91 aromatics remains elusive. Over the past decade, thanks to the development of nitrate-based

92 chemical-ionization atmospheric-pressure-interface long-time-of-flight mass spectrometers

93   (nitrate-CI-APi-LToF), there have been significant advancements in the detection of highly

94   oxygenated organic molecules and radicals, which is crucial for elucidating the mechanisms of

95   Cl-initiated reactions with VOCs (Bianchi et al., 2019; Ehn et al., 2010). The formation of

96   highly oxygenated organic products, including Cl-containing ones from the reactions of

97   biogenic VOCs with Cl atoms, were gradually revealed, whereas whether or not significant

98   amounts of Cl-containing highly oxygenated organics and radicals can be formed from Cl atoms

99   and aromatics remains unclear (Wang et al., 2020).

100 OOMs can lead to potential air quality, climate, and health effects. Due to their low volatility,

101 OOMs have been identified as dominant precursors for the growth of newly formed particles

102 and formation of SOAs, which are known for their negative effect on air quality and climate

103 impacts (Ehn et al., 2014; Kulmala et al., 2013). Compared to non-chlorine-containing OOMs

104 (non-Cl-OOMs), Cl-OOMs formed through the introduction of chlorine substituents make

105 organic compounds more lipophilic, facilitating their interactions with hydrophobic sites and

106 promoting enzymatic biotransformation in general, which can lead to adverse health effect in

107 turn (Henschler, 1994; Zhang et al., 2019). Therefore, field and laboratory studies for

108 characteristics and sources of Cl-OOMs from the reactions of Cl-aromatics and their risk

109 assessment upon human atmospheric exposure should be carried out.

110 In this study, we investigated non-Cl-OOMs and Cl-OOMs formation mechanisms from Cl-

111 initiated reactions of toluene, m-xylene, and 1,2,4-trimethylbenzene (1,2,4-TMB) in the

112 presence and absence of NO_x in a laboratory flow reactor, using a nitrate-CI-APi-LToF

113 (Aerodyne Research, Inc. USA, and Tofwerk AG, Switzerland) and a Vocus proton-transfer-

114 reaction long-time-of-flight mass spectrometer (Vocus-PTR-LToF) (Tofwerk AG,

115 Switzerland). In addition, the nitrate CI-APi-LToF was also deployed in a field campaign in

116 suburban Shanghai during winter to search for ambient gaseous Cl-OOMs. The toxicity of

117 selected Cl-OOMs, which were simultaneously detected both in laboratory experiments and

118 ambient observations, was evaluated by computational toxicity.

119 **2. Materials and methods**

120 **2.1. Experimental Set-up in the Laboratory.**

121   A general scheme of the experimental setup is shown in Figure S1. Simulation experiments

122   were conducted in a 6 L quartz flow tube reactor with a total flow rate of 10 L min^{-1}, resulting

123   in a residence time of ~36 seconds. This flow tube is covered by aluminum composite panels

124   to avoid room light. Zero air with relative humidity (RH) less than 1% generated from a Zero

125   Air Generator (AADCO Instruments, Inc. USA) was used as carrier gas. The reaction

126   temperature was maintained at around 20°C.

127   Homemade aromatics–N_2 cylinders were prepared from their liquid standards (toluene, ≥

128   99.0%, Aladdin; m-xylene, ≥ 99.0%, Aladdin; 1,2,4-TMB, ≥ 99.5%, Aladdin) together with

129   high-purity nitrogen gases. Cl atoms were produced by photolysis of chlorine (Cl_2, Shanghai

130   Wetry Standard Reference Gas Analytical Technology Co., LTD) using 350 nm UV lights. In

131   experiments with NO_x, NO (Air Liquid Co., LTD) was added into the flow tube to produce and

132   sustain NO_x mixing ratios that were sufficiently high to be a competitive sink for RO_2 radicals.

133   RH is controlled by changing zero air flowrates through the water bubbler. Before each

134   experiment, the wall of the flow tube was cleaned with a water/alcohol solution and then purged

135   with zero air for over 1 hour. Details of the experimental setup are provided in Text S1 of the

136   Supporting Information.

137   The concentration of Cl atoms was controlled by adjusting the flow rate of Cl_2. The mean

138   concentrations of Cl atoms were determined according to the decay of aromatic precursors

139   (Figure S2) and calculated using Eq.(1), with reaction rate coefficients k of 6.2×10^{-11} cm^3

140   molecule^{-1} s^{-1}, 1.35×10^{-10} cm^3 molecule^{-1} s^{-1}, and 2.42×10^{-10} cm^3 molecule^{-1} s^{-1} for reactions

141   between Cl atoms and toluene, m-xylene, and 1,2,4-TMB, respectively(Wang et al., 2005), as

142   follows:

143   $$[Cl] = -1/kt \times \ln([Aromatics]_t/[Aromatics]_0) \qquad \text{Eq.} (1)$$

144   where $[Aromatics]_0$ and $[Aromatics]_t$ are the initial concentration and the concentration

145   after a reaction time t of aromatic precursors, respectively. $[Cl]$ is the estimated concentration

146   of Cl atoms in the flow tube. In our flow tube experiments, the extent of oxidation is quantified

147   using the parameter of Cl exposure, defined as $[Cl]$ multiplied by the reaction time t. Cl

148   exposures in our experiments were in the range of $(1.2-2.0) \times 10^9$ molecules cm^{-3} s, equivalent

149 to atmospheric oxidation times of roughly 0.6-1.3 hours for aromatics at a daytime Cl atom

150 concentration of 5×10^5 molecules cm^{-3} (Chang et al., 2004; Tham et al., 2016; Wang et al.,

151 2023).

152   A Vocus-PTR-LToF and a nitrate-CI-APi-LToF (more details refer to Text S2 & Figure S3

153 in Supporting Information) were simultaneously deployed to detect aromatic precursors and

154 gaseous OOM products, respectively. In addition, an iodide-CIMS (I-CIMS, Tofwerk AG,

155 Switzerland) was used in a separate experiment focusing on the m-xylene + Cl system to expand

156 the detection of Cl-initiated reaction products. Their working principles were described in

157 details elsewhere (Eisele and Tanner, 1993; Krechmer et al., 2018). Signals of aromatic

158 precursors and reaction products measured from the zero air were treated as their background.

159 The resolving power of the nitrate CI-APi-LToF was up to around 8000 for ions with m/z larger

160 than 200 Th. The ions of NO_3^-, $HNO_3 \cdot NO_3^-$, and $C_6H_5NO_3 \cdot NO_3^-$ were selected for mass

161 calibration, and the calibration error is less than 1ppm. When identifying the OOM signal peaks,

162 the error is limited below 4 ppm.

163   OOM concentrations are estimated by Eq. (2)(Kürten et al., 2016),

$$[OOMs] = C \times \frac{OOM \cdot NO_3^-}{NO_3^- + HNO_3 \cdot NO_3^- + (HNO_3)_2 \cdot NO_3^-} \times T \qquad \text{Eq. (2)}$$

164

165 where $OOM \cdot NO_3^-$, NO_3^-, $HNO_3 \cdot NO_3^-$, and $(HNO_3)_2 \cdot NO_3^-$ represent signals of corresponding

166 ions in units of counts per second (cps). OOMs with an oxygen content of equal to or more than

167 6 (i.e., highly oxygenated organic molecules, HOMs) are assumed to cluster with NO_3^- at the

168 same rate coefficient as that of sulfuric acid (H_2SO_4), i.e., both at collision-limited rates

169 (Bianchi et al., 2019; Ehn et al., 2010). Therefore, the calibration factor C for sulfuric acid is

170 adopted as that of OOMs (Kürten et al., 2011, 2012). It should be noted we also used the same

171 calibration factor C for quantification of OOMs with an oxygen number of less than 6, which

172 may lead to relatively high uncertainties (Alage et al., 2024). A mass-dependent transmission

173 correction factor T of our instrument is also taken into account in this study (Heinritzi et al.,

174 2016). The mass-dependent transmission correction factor is instrument-specific and

175 determined by depleting the primary ion with a series of perfluorinated acids and comparing

176 the primary ion signal depletion with the product signal increase (which would match for

177 equivalent transmission efficiency) (Lu et al., 2020).

178 In addition, a NO_x monitor (Thermo, 49i) was utilized to measure NO_x concentrations in

179 laboratory experiments. A nano-SMPS (Scanning Mobility Particle Sizer with a nano

180 Differential Mobility Analyzer, TSI, USA) together with a PSM (Particle Size Magnifier,

181 Airmodus, Finland) were used to detect particles in the range of sub-3 nm to 60 nm, indicating

182 the absence of newly formed particles during all experiments.

183 Table 1 summarizes experimental conditions including mixing ratios of aromatic precursors

184 (i.e., toluene, m-xylene, and 1,2,4-TMB), NO_x, and RH.

185   **Table 1.** Summary of experimental conditions in the laboratory experiments.

Exp.	Precursor	Initial precursor concentration (ppb)	Initial NO [a] (ppb)	Estimated Cl exposure ($\times 10^9$ molecule cm^{-3} s)	RH [b] (%)	Non-Cl-OOMs molar yield (%)	Cl-OOMs molar yield (%)	Ratio (Cl-OOMs/ Total OOMs, %)	Ratio (Dimer/ Monomer, %) [c]
1	Toluene	80	0	2.0	<1	5.1	2.4	32	3.5
2	Toluene	80	0	1.2	60	0.7	0.3	31	2.0
3	Toluene	84	45	2.7	<1	6.8	2.6	28	1.7
4	Toluene	80	40	1.6	60	1.8	0.8	29	1.0
5	m-Xylene	87	0	2.0	<1	0.6	0.5	43	3.2
6	m-Xylene	87	0	1.6	68	0.3	0.2	44	2.6
7	m-Xylene	90	45	1.7	<1	1.4	0.6	31	0.9
8	m-Xylene	87	50	2.3	35	1.1	0.5	32	1.2
9	1, 2, 4-TMB	98	0	1.4	<1	0.5	0.3	34	2.1
10	1, 2, 4-TMB	103	0	1.4	30	0.3	0.2	35	1.4
11	1, 2, 4-TMB	93	40	2.2	<1	1.5	0.7	31	0.8
12	1, 2, 4-TMB	109	55	2.2	30	1.0	0.6	37	0.6

186   [a] In the presence of NO experiments, there is more OH chemistry was involved in Cl-aromatics reactions and its influence can lead to relatively high uncertainty in the

187   molar yields reported in the table for pathways influenced by OH chemistry. Approximately 90% of NO was converted into NO$_2$ after the UV light was turned on.

188   [b] Relative humidity.

189   [c] The molar yield ratios of total OOM dimers to monomers. Monomers are defined as molecules with a carbon number equal to the carbon number of aromatic precursor

190   (nC), and dimers are defined as molecules with carbon numbers ranging from 2nC -1 to 2nC +1.

2.2. Field measurements.

A field campaign was conducted from December 14th, 2022, to February 2nd, 2023, at the Dianshan Lake (DSL) Air Quality Monitoring Supersite in suburban Shanghai, China (31.10°N,120.98°E). This monitoring site is frequently impacted by regional transport and experiences episodes of anthropogenic pollution. A detailed description of this site can be found elsewhere (Wu et al., 2023; Yang et al., 2022, 2023). A Vocus-PTR-LToF and a nitrate-CI-APi-LToF were both deployed in this field campaign to detect aromatics and Cl-OOMs, respectively. The detailed description of nitrate-CI-APi-LToF and Vocus-PTR-LToF, and their calibration in the field measurement are shown in the Supporting Information (Text S2).

2.3. Heath effect estimation.

A number of Cl-OOMs were assessed using the Estimation Program Interface Suite (EPI, V. 4.11) and Toxicity Estimation Software Tool (T.E.S.T, V. 5.1.2) software provided by the United States Environmental Protection Agency (EPA), to estimate their persistence, bioaccumulation, and toxicity through calculated half-life for reactions with OH, bioconcentration factors (BCF), oral rat pLD_{50} (-log10(pred), mol/kg), developmental toxicity, and mutagenicity. The models utilized the SMILES (Simplified Molecular Input Line Entry System) notation of the target compounds as input for the prediction.

3. RESULTS AND DISCUSSION

3.1. OOM molar yields.

The molar yields of OOMs are determined as OOMs formed (ΔM, molar cm^{-3}) divided by precursor reacted (ΔAr, molar cm^{-3}):

$$Molar\ yield = \frac{\Delta M}{\Delta Ar} \qquad \text{Eq. (3)}$$

Table 1 summarizes non-Cl-OOMs' and Cl-OOMs' molar yields and OOMs' dimer-to-monomer ratios from our laboratory experiments. The molar yields of non-Cl-OOMs and Cl-OOMs from reactions of three aromatic precursors with Cl atoms in the absence of NO_x are within the ranges of 0.3-5.1% and 0.2-2.4%, respectively. These values are comparable with previously reported: HOM molar yields (0.8-4.0%) detected by nitrate-CI-APi-LToF for the reactions between α-

218 pinene and Cl atoms (Wang et al., 2020) and non-Cl-OOMs molar yields (4.4-8.8%) detected

219 by H_3O^+-Chemical Ionization Mass Spectrometry (H_3O^+-CIMS) for the reactions between m-

220 xylene and Cl atoms (Bhattacharyya et al., 2023). The low molar yields observed in both this

221 study and previous studies may be attributed to the preference of different detection techniques.

222 Nevertheless, the observed ratio of Cl-OOMs to non-Cl-OOMs, ranging from 29% to 44%

223 (Table 1), further indicates the non-negligibility of the Cl-OOMs products among the total

224 OOMs products. In the presence of 40-55 ppb NO_x, our flow tube experiments show that the

225 molar yields of non-Cl-OOMs and Cl-OOMs from three aromatics are within the ranges of 1.0-

226 6.8% and 0.5-2.6%, respectively. The addition of NO_x can slightly increase the molar yields of

227 both non-Cl-OOMs and Cl-OOMs.

228   Typically, the fate of peroxy radicals in flow tube experiments is largely influenced by their

229 reactions with other RO_2, HO_2, or NO species, which are contingent upon the specific

230 experimental conditions (Bianchi et al., 2019; DeMore et al., 1997). In experiments without

231 NO_x, while the termination of RO_2 was primarily anticipated to be governed by RO_2-RO_2 and

232 HO_2-RO_2 reactions. However, after the addition of NO_x, the reaction between RO_2 and NO

233 tended to predominate, leading to a reduction in the dimer-to-monomer ratio by 50.5% (Exp. 3

234 and Exp. 1 in Table 1).

235   In contrast to OH reaction, the presence of Cl, ClO, and Cl_2 in chlorine-involved reaction

236 may introduce additional reaction pathways related to Cl-OOM formation. However, these

237 pathways make only minor contributions to the formation of Cl-OOMs under our experimental

238 conditions (see Text S4 in Supporting Information for detailed analysis).

239   Although both the non-Cl-OOMs and Cl-OOMs molar yields increased in the presence of

240 NO_x, the ratio of Cl-OOMs to the total OOMs decreased when NO_x was added. This

241 phenomenon can be attributed to the significant contribution of OH chemistry, primarily

242 resulting from the NO + HO_2 reaction. The additional OH radicals can contribute to the

243 formation of non-Cl-OOMs, as supported by recent experimental and modeling studies on the

244 reaction dynamics between Cl atoms and isoprene (Wang et al., 2022). For our experiments, as

245 NO_x was added into the flow tube, the concurrent presence of Cl atoms, OH radicals, and

246 aromatics led to a notable increase in the total OOM molar yields, ranging from 25 to 187%,

247 while reducing the ratios of Cl-OOMs to the total OOMs by approximately 9-28% (Table 1).

248 In addition, the increased Cl-OOM yields under NO_x conditions may result from the

249 suppression of dimer or multimer formation (Table 1), which shifts the product distribution

250 toward monomeric Cl-OOMs and thus leads to potential higher apparent yields. Moreover,

251 NO_x-promoted chemistry facilitates the formation of nitrogen-containing OOMs with diverse

252 structures and functionalities. The nitrate-CI-APi-LToF exhibits different detection sensitivities

253 toward these species, which may also influence the estimated molar yields under high NO_x

254 conditions. Besides, high RH leads to low molar yields, which may be attributed to the

255 depressed detection efficiency of OOMs and the elevated vapor wall loss under humid

256 conditions (Huang et al., 2018). The product distribution remains unchanged under high

257 humidity conditions (see Figure 1B and Figure S4), indicating that the presence of water does

258 not significantly influence the reaction between Cl atoms and aromatics.

259 **3.2. Characteristics of OOM products and peroxyl radicals.**

260 Mass defect plots of stabilized products from reactions between toluene (Exp.1 in Table1),

261 m-xylene (Exp.5 in Table1), and 1,2,4-TMB (Exp.9 in Table1) and Cl atoms in the absence of

262 NO_x are shown in Figure 1. These products display similar distribution patterns, consisting of

263 monomers (with carbon numbers equal to carbon numbers of the precursor, nC) and dimer

264 products (with carbon numbers ranging from 2nC -1 to 2nC +1). The ratio of dimer products to

265 monomer products are 3.5%, 3.2%, and 2.1% for reactions of toluene, m-xylene, and 1,2,4-

266 TMB with Cl atoms, respectively. Meanwhile, the products also can be classified into two

267 groups: non-Cl-OOMs in blue and Cl-OOMs in orange in Figure 1. In general, the total

268 concentration of Cl-OOMs is lower than that of non-Cl-OOMs. Specifically, the concentrations

269 of Cl-OOMs account for 47%, 91%, and 52% of the non-Cl-OOMs in the toluene, p-xylene,

270 and 1,2,4-trimethylbenzene experiments, respectively. Both non-Cl-OOMs and Cl-OOMs

271 products can be categorized into several bands, as indicated by the dashed lines in Figure 1,

272 each of which comprises compounds with varying numbers of oxygen atoms.

273

274
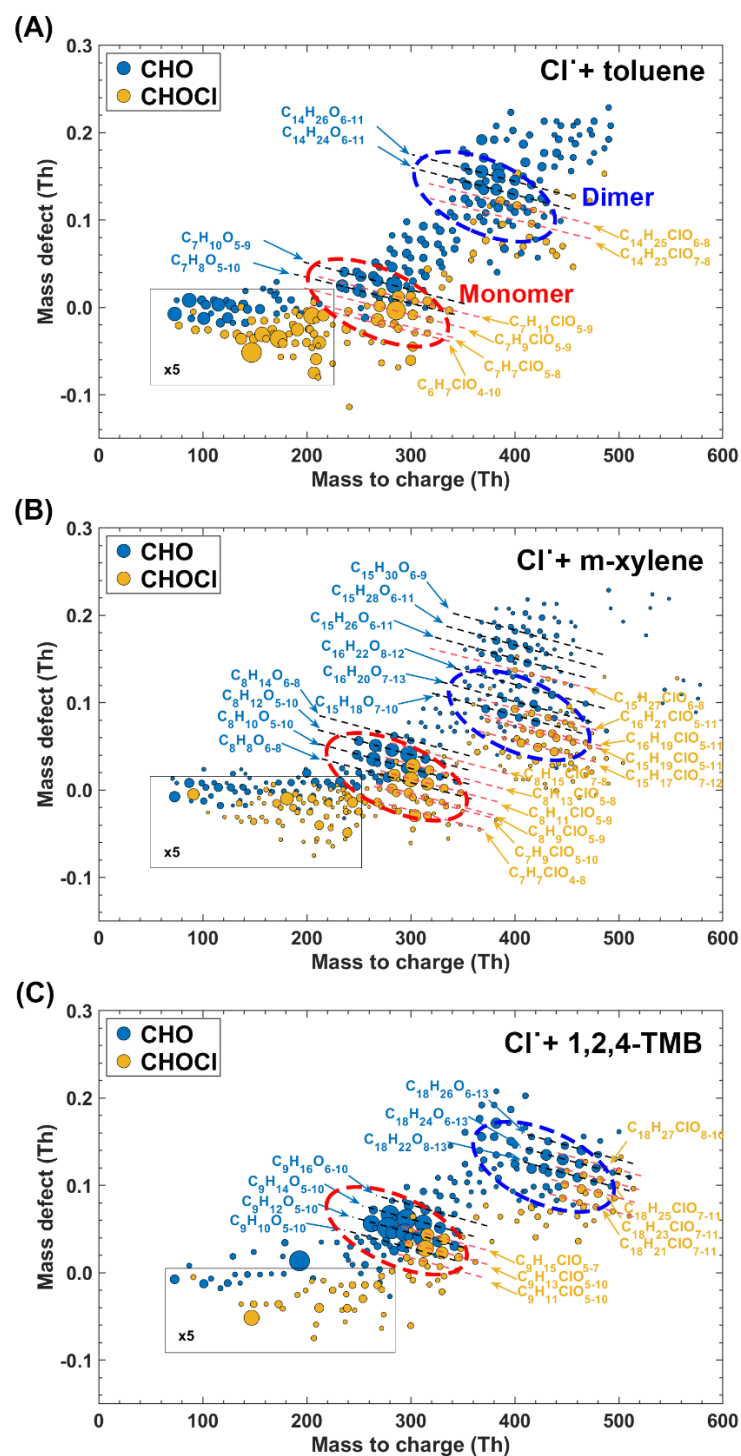
Figure 1. Mass defect plots of OOM products detected by a nitrate-CI-APi-LTOF from Cl-initiated reactions of (A) toluene, (B) m-xylene, and (C) 1,2,4-trimethylbenzene, respectively, in the absence of NO_x. The detected products are marked by their exact mass (with NO_3^- reagent ions) and mass defect (exact mass subtracted by its unit mass). The lines annotate the general chemical formulae. Chlorine-containing and non-chlorine-containing formulae are shown in different colors. The size of the circle corresponds to the concentration of products.

280 The mass spectrum of the detected OOMs monomer and dimer products from the reaction

281 between m-xylene and Cl atoms with and without NO_x (Exp. 5&7 in Table 1) are shown in

282 Figure 2. Without NO_x, dominant monomer products for non-Cl-OOMs included $C_8H_{10}O_6$ and

283 $C_8H_{12}O_{6-8}$, whereas for Cl-OOMs, $C_8H_{11}ClO_{6-8}$ and $C_8H_{13}ClO_{6-7}$ dominated. The most

284 abundant dimer compounds for non-Cl-OOMs were $C_{16}H_{20}O_9$, $C_{16}H_{22}O_{10}$, and $C_{15}H_{18}O_8$,

285 whereas for Cl-OOMs, $C_{16}H_{19}ClO_{8,10}$, $C_{16}H_{21}ClO_9$, and $C_{15}H_{17}ClO_8$ prevailed. Dimer products

286 containing two Cl atoms were also observed, exemplified by $C_{16}H_{18,20}Cl_2O_{10}$. Under NO_x-

287 present conditions, the main non-Cl-OOMs included $C_8H_{11}NO_{6-10}$ and $C_8H_{12}N_2O_{10}$, whereas

288 Cl-OOMs were represented by $C_8H_{10}ClNO_{7-8}$ and $C_8H_{11}ClN_2O_{9-10}$.

289
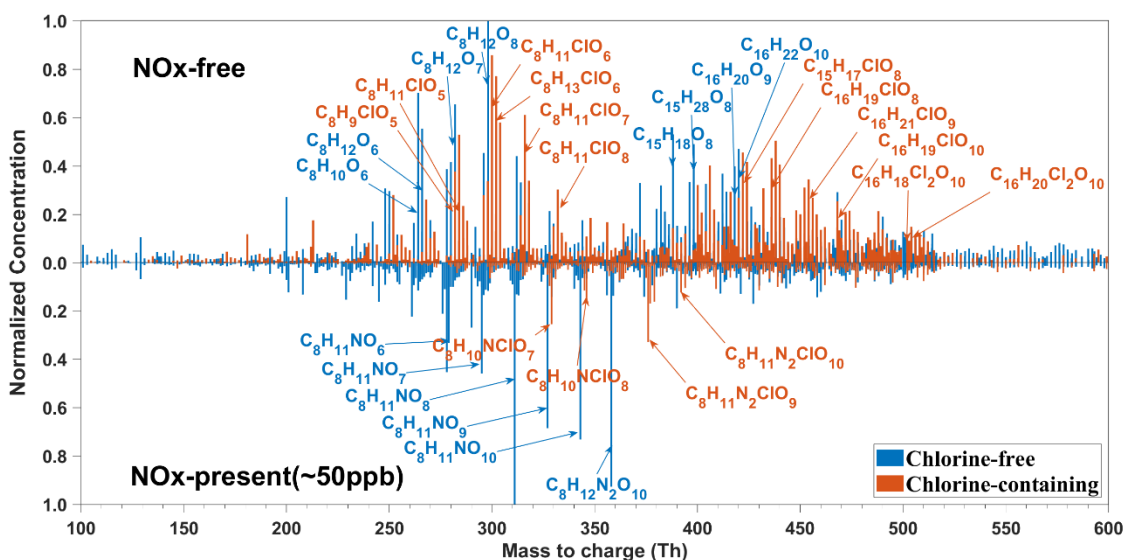
291 **Figure 2.** Mass spectra of OOM products detected by a nitrate-CI-APi-LToF from the reaction of m-xylene and
292 Cl atoms under NO_x-free and NO_x-present conditions. The y-axes in both figures are standardized by setting their
293 maximum concentrations to 1.

294 Moreover, 29 peroxyl radicals in total were observed in our flow tube experiments with

295 three precursors, as listed in Table S1 and illustrated in Figures 3 & S5. It is crucial to note,

296 however, that not every intermediate radical formed could be conclusively identified. This is

297 primarily due to the inherent instability and the extremely brief life span of peroxyl radicals,

298 which pose significant challenges for their detection. Currently, the absolute concentrations of

299 radicals measured by I-CIMS cannot be reliably quantified. Therefore, for visualization and

300 comparative purposes, the signal intensities of the radicals $C_8H_{10}ClO_{2-3}$ detected by I-CIMS

301 were normalized to match the signal intensity of $C_8H_{10}ClO_4$ measured by nitrate-CI-APi-LToF,

302 as presented in Figure 3. It is essential to note that this normalization was solely used to facilitate

303 consistent visual comparison across instruments. Consequently, the normalized I-CIMS signals

304 are not utilized for quantitative comparisons of radical concentrations in the subsequent

305 discussion.

306
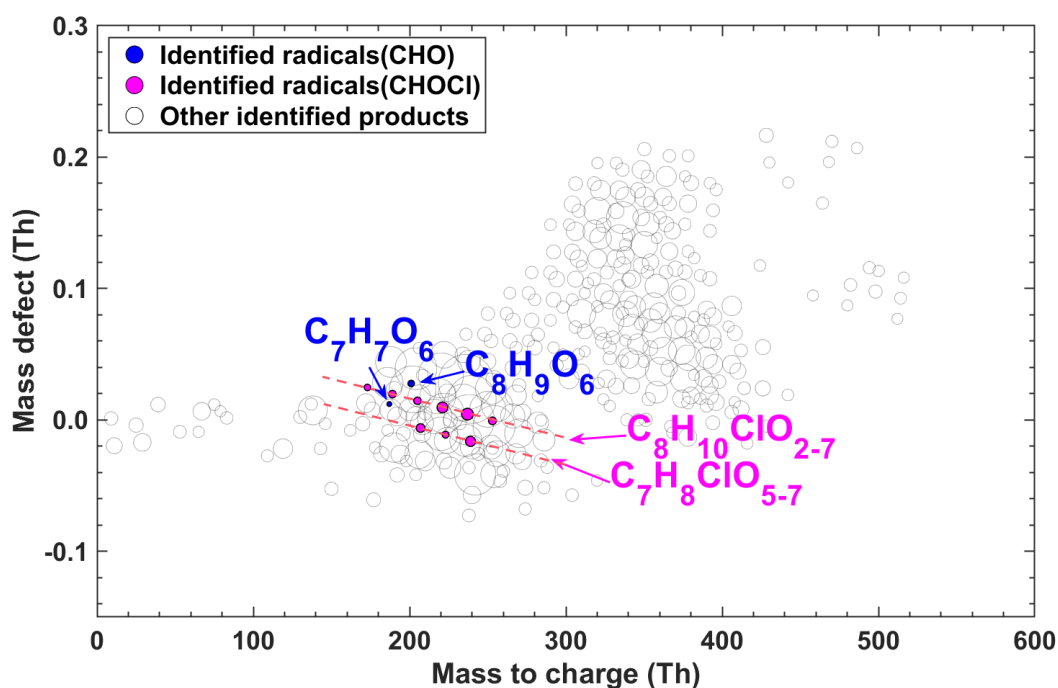
Figure 3. Mass defect plot of peroxyl radicals detected by a nitrate-CI-APi-LToF and an I-CIMS from Cl-initiated
reactions of m-xylene without NO_x. $C_8H_{10}ClO_{2-3}$ were detected by I-CIMS while the remaining radicals were
observed using nitrate-CI-APi-LToF. The detected products are marked by their exact mass (with NO_3^- reagent
ions) and mass defect (exact mass subtracted by its unit mass). The lines annotate the general chemical formulas.
Chlorine-containing and non-chlorine-containing formulas are shown in different colors. The size of the circle is
proportional to the concentrations of peroxyl radicals.

313 Take the reaction between Cl atoms and m-xylene in the absence of NO_x for example, we

314 detected peroxyl radicals including $C_8H_{10}ClO_{2-7}$, $C_7H_8ClO_{5-7}$, $C_8H_9O_6$, and $C_7H_7O_6$ (Figure 3

315 & Figure S5). High-resolution peak fittings of partial peroxy radicals from the raw mass

316 spectrum obtained by nitrate-CI-APi-LToF are shown in Figure S6. Notably, the dominant

317 species among these radicals was $C_8H_{10}ClO_6$, constituting 27.4% of the total signal of identified

318 peroxyl radicals in the reaction of Cl atoms and m-xylene and nearly three times of the $C_8H_9O_6$

319   radical signal. Also, similar ratio rules of chlorine-containing radicals (analogy of $C_8H_{10}ClO_6$)

320   to non-chlorine-containing radicals (analogy of $C_8H_9O_6$) were observed for toluene (~4.2 times)

321   and 1,2,4-TMB (~3.8 times). Although $C_7H_8ClO_{5-7}$ radicals were also discernible, their signal

322   intensity was merely 22.3% of the total signal of identified peroxyl radicals in the reaction of

323   Cl atoms and m-xylene. Non-Cl-containing radicals were also detected, albeit with substantially

324   lower signal values, accounting for only 15.5% of the total identified radical signals.

325 **3.3. Formation mechanisms of Cl-OOMs**

326 **3.3.1. Cl-addition pathway**

327   Given the similar product patterns for the three precursors (toluene, m-xylene, and 1,2,4-

328   TMB), it is reasonable to infer that the reaction mechanisms between different aromatics and

329   Cl atoms are analogous. A generalized mechanism is thus proposed, elucidating the Cl-initiated

330   reactions of m-xylene in the absence of NOx, as depicted in Scheme 1. This scheme serves as

331   a representative example highlighting the potential pathways involved in the Cl-initiated

332   reactions of aromatics.

333
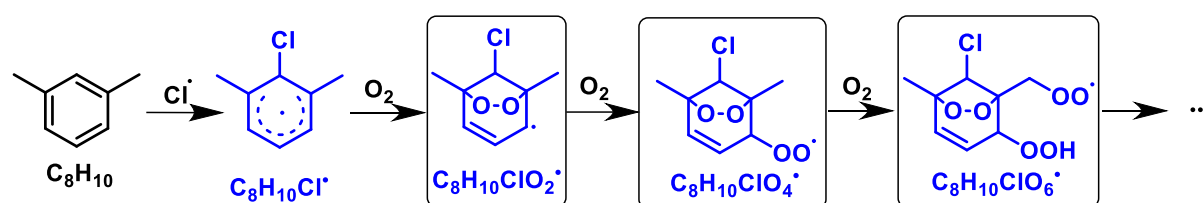
335 **Scheme 1.** Proposed reaction mechanisms of m-xylene with Cl atoms leading to the formation of Cl-OOMs.
336 Radicals detected by nitrate-CI-APi-LToF are marked with black boxes.

337   Although the theoretical studies by Huang *et al.* (2012) show that the Cl-addition pathway

338   accounts for only 14% of Cl-initiated reactions of toluene (298K), which is significantly lower

339   than the 86% attributed to the H-abstraction pathway, the proportion of Cl-OOMs products

340   from Cl-addition reaction should not be overlooked, as evidenced by the observation of peroxyl

341   radicals and product distribution characteristics in this study (Huang et al., 2012). The initial

342   reaction of m-xylene (C_8H_{10}) with Cl atoms can occur through two pathways: the Cl-addition

343   pathway, leading to the formation of a $C_8H_{10}Cl$ radical ($C_8H_{10}Cl\cdot$, refer to Scheme 1) or the H-

344 abstraction pathway, forming a C_8H_9 radical ($C_8H_9\cdot$, refer to Scheme S1) and C_8H_9 radical

345 ($C_8H_9O_2\cdot$ refer to Scheme S1). Then, both $C_8H_9\cdot$ and $C_8H_{10}Cl\cdot$ can in turn undergo autoxidation

346 via the H-shift and addition of O_2 to produce peroxy radicals of $C_8H_{10}O_5\cdot$ or

347 $C_8H_{10}ClO_6\cdot$ (Vereecken and Nozière, 2020; Bianchi et al., 2019). The peroxyl radical

348 $C_8H_{10}ClO_6\cdot$ was identified as the predominant species in terms of signal (Table S1). Although

349 these Cl-OOMs-to-non-Cl-OOMs signal ratios may not accurately represent their relative

350 concentrations due to sensitivity differences of these radicals towards the reagent ions

351 (($HNO_3)_{0-1}\cdot NO_3^-$), it is still noteworthy that these Cl-RO_2 overlooked in previous studies were

352 directly observed in such a reaction system, thereby suggesting that Cl-addition pathway is

353 indeed present in the initial reaction steps of reactions between Cl atoms and aromatics.

354   In the reaction of Cl atoms and m-xylene, a certain fraction of the peroxyl radicals

355 ($C_8H_{10}ClO_6\cdot$) might also be derived from the secondary Cl-addition reaction between Cl atoms

356 and a first-generation stabilized product $C_8H_{10}O_6$ (Scheme 1). Indeed, it is challenging to

357 evaluate the exact contribution from secondary Cl-addition reaction to the formation of

358 $C_8H_{10}ClO_6\cdot$. However, it may be indirectly assessed via the potential secondary reactions

359 between more dominant first-generation stabilized products ($C_8H_{12}O_x$) and Cl (Table S2), since

360 $C_8H_{10}O_6$ and $C_8H_{12}O_x$ likely react with Cl at similar rates. If secondary Cl-addition reactions

361 were significant in the reaction system of Cl atoms and m-xylene, $C_8H_{12}O_x$ should undergo

362 secondary Cl-addition reactions to generate $C_8H_{12}ClO_x$ radicals. Yet, $C_8H_{12}ClO_x$ radicals were

363 not detectable, which hints that secondary Cl-addition reactions could only play a minor role in

364 our experiments. Therefore, it appears that the secondary Cl-addition reactions between

365 stabilized products and Cl atoms are less significant compared with Cl-addition in the initial

366 reaction steps.

367   Recently, Jahn et al. (2024) investigated the formation of secondary organic aerosols from

368 the reaction of ethylbenzene and Cl atoms, and attributed the observed Cl-addition products to

369 reactions involving non-aromatic C=C bonds (Jahn et al., 2024). They claimed that OH radical

370 existed in their experiments, due to the presence of NOx. As a result, approximately 40% of

371 ethylbenzene reacted with Cl atoms, 30% with OH, and 30% remained unreacted. Thus, a

372 secondary Cl addition to $C_8H_{11}NO_6$ for reaction of ethylbenzene and Cl atoms, forming

373 $C_8H_{12}ClNO_8$, is possible (Scheme S1). In our experiments, although OH radicals can still be

374 generated through H-abstraction from methyl groups by HO_2 (Bhattacharyya et al., 2023), the

375 use of 20 ppm CO as an OH scavenger confirmed the presence of OH chemistry in our system.

376 Nevertheless, the stable real-time signals of first-generation products and radicals from the Cl-

377 addition reaction, observed both with and without OH chemistry, provide compelling evidence

378 that the Cl-addition pathway remains the dominant mechanism for Cl-RO_2 formation under

379 low-NO_x conditions (see Text S5 in the Supporting Information). Moreover, under high NO_x

380 conditions in our experiments, the dominant Cl-OOMs $C_8H_{10}ClNO_7$ (Scheme S2), contains two

381 fewer H atoms than the $C_8H_{12}ClNO_8$ proposed by Jahn et al. (2024) as a secondary Cl-addition

382 product (Scheme S3). While this difference might suggest the presence of an additional double

383 bond or a ring in $C_8H_{10}ClNO_7$, it could also result from multi-generation oxidation chemistry.

384 Specifically, H-abstraction from a carbon bearing an OH or OOH can form a carbonyl, thereby

385 reducing the hydrogen count without requiring a new double bond.

386 **3.3.2. Autoxidation and subsequent reactions of Cl-RO_2**

387 Scheme 2 shows a proposed reaction mechanism for the autoxidation of the main Cl-RO_2

388 radical ($C_8H_{10}ClO_4\cdot$) generated from Cl atoms and m-xylene. Autooxidation of $C_8H_{10}ClO_4\cdot$

389 leads to $C_8H_{10}ClO_6\cdot$. There are two distinct isomeric forms of $C_8H_{10}ClO_6\cdot$, denoted as

390 $C_8H_{10}ClO_6\cdot$(I) and $C_8H_{10}ClO_6\cdot$(II), which is similar to results for aromatics + OH by Molteni

391 et al (Molteni et al., 2018). Notably, the formation of $C_8H_{10}ClO_6\cdot$(II) requires a second step of

392 endo-cyclization, which is not competitive on account of its slow reaction rate, as inferred from

393 several previous studies using both experimental and theoretical approaches of OH-initiated

394 oxidation of aromatics (Wang et al., 2017; Xu et al., 2020). Therefore, the abundance of

395 $C_8H_{10}ClO_6\cdot$(I) would likely be much higher than $C_8H_{10}ClO_6\cdot$(II), and our following discussion

396 primarily focuses on the subsequent reaction processes involving $C_8H_{10}ClO_6\cdot$(I). Briefly,

397 $C_8H_{10}ClO_6\cdot$ reacts with $RO_2\cdot$ to generate $C_8H_{9,11}ClO_5$ and $C_8H_{10}ClO_5\cdot$ (Reaction pathway *R2b*)

398 and with an HO_2 radical to produce $C_8H_{11}ClO_6$ (Reaction pathway *R2c*). Meanwhile,

399 $C_8H_{10}ClO_6\cdot$ has no more H atoms for another H-shift at an appreciable rate based on our current

400 understanding.(Wang et al., 2024) In the presence of NO_x, $C_8H_{10}ClO_6\cdot$ is terminated (Reaction

401 pathway *R2a*), leading to the formation of $C_8H_{10}ClNO_7$ products.

402
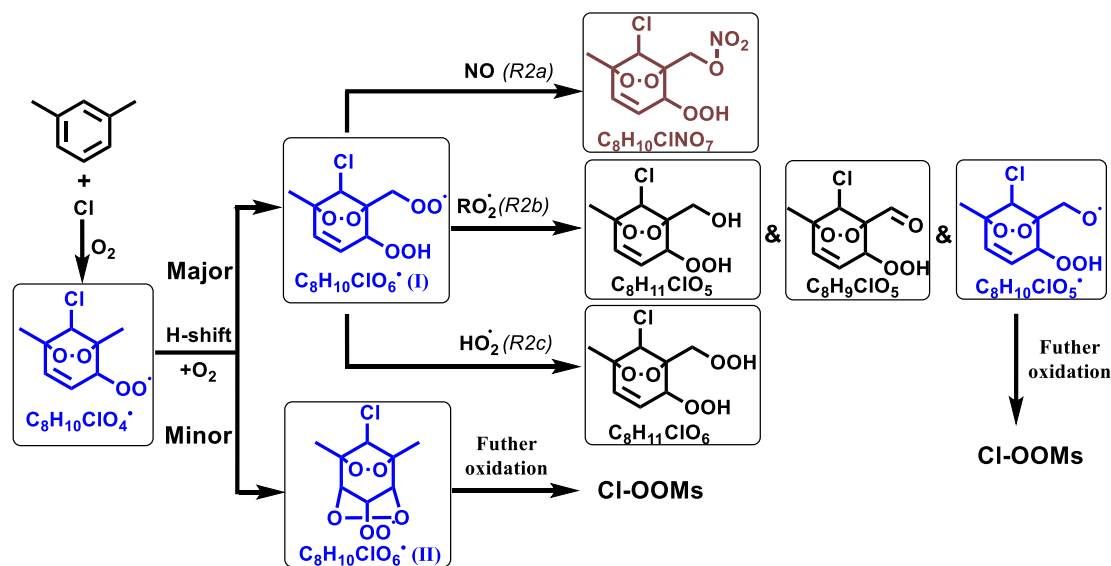
Scheme 2. Reaction pathways of the bicyclic peroxyl radical $C_8H_{10}ClO_4$ in the Cl-initiated reaction of m-xylene.
404 Blue, brown, and black formulae denote radicals, nitrogen-containing products, and Cl-OOMs products,
405 respectively. Radicals and stable products detected by nitrate-CI-APi-LToF are marked with black boxes.

3.3.3. Dimer formation

407 The accretion reaction ($RO_2 + R'O_2 \rightarrow ROOR' + O_2$) represents a pivotal source for dimer

408 compounds, originating from highly oxidized and functionalized RO_2 radicals (Ehn et al., 2014;

409 Zhao et al., 2018). As shown in Figure 2, $C_{16}H_{19}ClO_8$ and $C_{16}H_{19}ClO_{10}$ are two typical accretion

410 reaction products from reactions between Cl atoms and m-xylene without NO_x. In detail,

411 $C_{16}H_{19}ClO_{10}$ can be formed through the accretion reaction between $C_8H_{10}ClO_6\cdot$ and $C_8H_9O_6\cdot$

412 (Scheme 3). The formation pathways for $C_{16}H_{19}ClO_8$ are more varied compared to that of

413 $C_{16}H_{19}ClO_{10}$. It can be produced either via the accretion of a $C_8H_{10}ClO_6$ radical with a $C_8H_9O_4$

414 radical or through the reaction of a $C_8H_{10}ClO_4$ radical with a $C_8H_9O_6$ radical. Meanwhile,

415 $C_{16}H_{20}Cl_2O_{10}$, which is also detected during the reaction, can be formed via the accretion

416 reaction of two $C_8H_{10}ClO_6$ radicals.
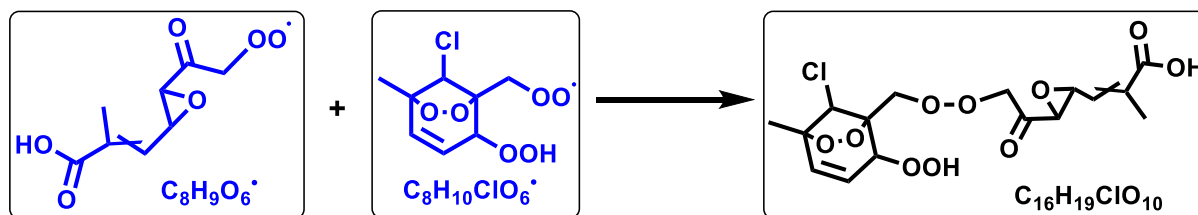
Scheme 3. Accretion reaction pathways of peroxyl radical $C_8H_{10}ClO_6\cdot$ and $C_8H_9O_6\cdot$ in the Cl-initiated reaction of m-xylene. Blue and black formulae denote radicals and stable products, respectively. Radicals and stable products detected by nitrate-CI-APi-LToF are marked with black boxes.

Previous studies have reported dimer formation rates during the OH-initiated oxidation of 1,3,5-trimethylbenzene, ranging from 1.4×10^{-10} to 25×10^{-10} cm^3 molecule^{-1} s^{-1} (Berndt et al., 2017). Compared to the OH reaction, $Cl-RO_2$ is produced in the Cl atom reaction, but its reaction rate in the accretion reaction remains unknown. If $Cl-RO_2$ have lower reactivity (i.e., slower rate coefficients) for accretion reactions compared to non-Cl-containing RO_2, the same generation rate of $Cl-RO_2$ and RO_2 would result in higher concentration of $Cl-RO_2$, resulting in the high $Cl-RO_2$ signal detected. However, the generation rate of both $Cl-RO_2$ and RO_2 are currently uncertain, further complicating the determination of the chemical mechanisms of Cl-initiated reactions even more challenging.

3.4. Cl-OOMs detection in suburban Shanghai.

As shown in Figure 4A and Table S3, a total of 51 gaseous Cl-OOMs were identified during winter in suburban Shanghai, whose high-resolution peak fittings measured by nitrate CI-APi-LToF are shown in Figure S7. Figure S8 further demonstrates the accuracy of our peak identification by showing the ratio of the fitted peak intensities versus the peak separation for identified Cl-OOM peaks and adjacent ions from our ambient nitrate-CI-APi-LToF measurements (Cubison and Jimenez, 2015). The peak separation, normalized to the half-width at half-maximum ($\chi = \Delta t/HWHM$), is greater than 1 for all Cl-OOMs. Notably, 22% of the peaks exhibit χ values between 1 and 2, indicating they are separable but closely spaced, while 78% of the Cl-OOMs ($\chi > 2$) are well-separated peaks.

Ambient Cl-OOMs consist of compounds mostly with a single Cl atom and only two with two Cl atoms. The carbon and oxygen numbers of these Cl-OOMs ranged from 2 to 14 and 1

442   to 11, respectively. Figure 4B shows the abundance distribution of gaseous Cl-OOMs on the

443   basis of carbon and oxygen numbers in their molecular formulae. Approximately 80%

444   concentration of the identified Cl-containing molecules is C5-C9 Cl-OOMs, among which C6-

445   C9 Cl-OOMs represent a large fraction of ~79 %. All assignments followed strict criteria for

446   mass accuracy (< 4 ppm) and isotopic pattern matching. Interference screening with adjacent

447   formulas (Table S4) was performed to ensure unambiguous identification. Nonetheless, the

448   detection of these low-oxygenated Cl-OOMs should be interpreted with caution, and we

449   acknowledge that their measured concentrations may carry higher uncertainty compared to

450   those of more oxygenated compounds.

451   38 Cl-OOMs observed in field measurements were also identified in our laboratory

452   experiments, corresponding to reaction products of Cl atoms with toluene, m-xylene, or 1,2,4-

453   TMB. These results indicate that ambient C6-C9 Cl-OOMs exemplified by $C_7H_7N_2ClO_9$,

454    $C_8H_{10}NClO_7$, and $C_9H_{15}ClO_8$ are likely formed from Cl-initiated reactions with aromatic

455   compounds. On the other hand, isoprene was considered as a precursor of C5 Cl-OOMs (Breton

456   et al., 2018; Priestley et al., 2018; Wang and Ruiz, 2017). Several relatively abundant ambient

457   Cl-OOMs, specifically $C_2H_2Cl_2O_2$, $C_6H_4ClNO_{3-4}$, $C_8H_7ClO_6$, and C_9H_6ClNO (Figure 4A),

458   although they were not observed in our flow tube experiments. The presence of $C_2H_2Cl_2O_2$

459   suggests possible contributions from the oxidation or atmospheric degradation of chlorinated

460   solvents, combustion emissions, or industrial processes (Wang et al., 2021). The $C_6H_4ClNO_{3-4}$

461   may originate from Cl-induced reaction of aromatics. Similarly, $C_8H_7ClO_6$ and C_9H_6ClNO

462   could be derived from more oxidized aromatic compounds undergoing multi-step oxidation or

463   fragmentation. The observation of these species highlights the complexity and diversity of Cl

464   chemistry in suburban environments, underscoring the importance of further studies integrating

465   broader precursor sets, longer aging times, and additional reaction pathways to better

466   understand their sources and formation mechanisms.

467   The diurnal profiles of all 51 Cl-OOMs identified in the ambient were shown in Figure S9.

468   Similar to previous reports in northern Europe and Beijing (Breton et al., 2018; Priestley et al.,

469   2018), Cl-OOMs increased with elevated solar radiation and their peaks appeared at around

470   12:00 p.m. (local time). This suggests that while ClNO$_2$ photolysis is a significant source of Cl

471   atoms in the early morning, and other sources such as the photolysis of Cl$_2$, ClONO$_2$, HCl, ICl,

472   and BrCl by sunlight can also contribute to Cl atom concentrations later in the day (Peng et al.,

473   2020). Besides, some Cl-OOMs could be formed through secondary reactions involving OH

474   radicals with Cl-VOCs or intermediates, rather than direct Cl atom-initiated reaction. While

475   distinguishing these pathways is beyond the scope of this study, the formation of Cl-OOMs is

476   likely influenced by both Cl- and OH-initiated mechanisms under ambient conditions,

477   especially in the presence of NO$_X$.

478
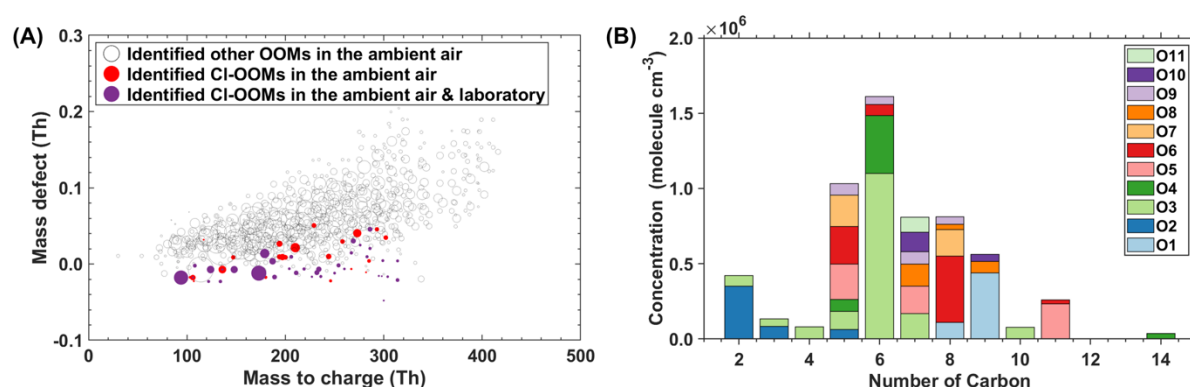
479   **Figure 4.** (A). Mass defect plot of detected OOMs by a nitrate-CI-APi-LToF in ambient air in suburban Shanghai.

480   Cl-OOMs only observed in the ambient atmosphere were marked in red, and Cl-OOMs observed in both ambient

481   and lab were marked in purple. The size of the circle is proportional to the concentration of compounds in the

482   ambient. (B). Distribution of carbon and oxygen number of gas-phase Cl-OOMs identified in suburban Shanghai.

483   The color codes correspond to the number of oxygen atoms.

484   **3.5. Health effect of ambient Cl-OOMs.**

485   Table S5 presents a detailed toxicity estimation of various Cl-OOMs, including C$_7$H$_7$N$_2$ClO$_9$,

486   C$_8$H$_{10}$NClO$_7$, and C$_9$H$_{15}$ClO$_8$, which were identified in the suburban Shanghai atmosphere and

487   laboratory experiments. These estimations are based on the potential chemical structures of

488   these Cl-OOMs. We characterized the toxicity of these Cl-OOMs using persistence,

489   bioaccumulative and toxic (PBT) criteria, as outlined in Table S5. Additionally, we conducted

490   a comparative analysis of their toxicity relative to that of naphthalene, a compound whose

491   atmospheric toxicity has been extensively studied.

492   Compounds with short OH radical reaction half-lives and bioconcentration factors (BCF) are

493   unlikely to be persistent and bioaccumulative. Among these Cl-OOMs, $C_8H_{10}NClO_7$ (II)

494   exhibits the slowest degradation rate with OH radicals with a half-life of 5 days, which suggests

495   that it is a potential new persistent pollutant (half-life > 2 days) in the atmosphere (Europe,

496   2023).

497   As indicated by the pLD_{50} values, toxicity levels of most Cl-OOMs are lower than that of

498   naphthalene, except for $C_8H_{10}NClO_8$, $C_8H_{10}NClO_7$ (I), and $C_7H_7N_2ClO_8$ (Table S5). Among

499   these compounds, $C_8H_{10}NClO_7$ (I) is identified with the highest predicted toxicity, followed by

500   compound $C_8H_{10}NClO_8$. The pLD_{50} of these compounds is categorized within level 3,

501   signifying their potential for a considerable acute toxicity.

502   Notably, the pLD_{50} values of Cl-OOMs are found to be akin to those of naphthalene.

503   However, given that their concentration in suburban Shanghai (0.55 ppt) is merely one percent

504   of that of naphthalene (50 ppt) as measured in this study, the total probabilistic hazard quotient

505   (PrHQ, defined as the product of estimated human exposure (ambient concentration) and pLD_{50}

506   in this study) of Cl-OOMs is lower. Despite this lower PrHQ, it is important to recognize that

507   each of the evaluated Cl-OOMs may pose risks of developmental toxicity and mutagenicity,

508   which underscores the need for a thorough understanding of the toxicological implications of

509   Cl-OOMs in the atmosphere.

4. Conclusions

510

511   In summary, this study highlights the Cl-addition-initiated reaction as a non-negligible

512   pathway in the reaction of Cl atoms with aromatics. Field measurements in suburban Shanghai

513   revealed 51 gaseous Cl-OOM species, with 38 of these Cl-OOMs also detected in our laboratory

514   experiments. This suggests that these Cl-OOMs likely derive from reactions between Cl atoms

515   and aromatics. Considering the significant role of Cl atoms in daily atmospheric oxidation

516   processes, overlooking the Cl-addition pathway could lead to ignoring the formation of Cl-

517   OOMs from aromatic compounds in the atmosphere. This study, therefore, highlights the

518   necessity of incorporating both pathways in the models for a more accurate assessment of the

519 atmospheric fate of Cl atoms and aromatics in urban settings. In addition, health effect

520 evaluation indicates that all assessed Cl-OOMs may possess developmental toxicity, and nearly

521 half of the compounds may exhibit carcinogenic effects. Considering the critical role of

522 aromatics in the urban air and recent observations reporting increased levels of reactive chlorine

523 species in polluted atmospheres, our study offers timely insights into the chemical processes

524 between Cl atoms and aromatics occurring in anthropogenically influenced atmospheres and

525 the adverse health effects of these Cl-containing reaction products.

526 **Data availability.**

527 The data used in this study are available upon request from Lei Yao (lei_yao@fudan.edu.cn)

528 and Lin Wang (lin_wang@fudan.edu.cn).

529 **Author contributions.**

530 LY and LW conceived and designed this study and revised the manuscript. CL analyzed and

531 interpreted data, drafted and revised the manuscript. CL and YW contributed to the modeling

532 of the data. MF and XC contributed to the health effect analysis.

533 **Competing interests.**

534 The contact author has declared that none of the authors has any competing interests.

535 **Financial support.** This research was supported by the National Key Research and

536 Development Program of China (2022YFC3704100) and the National Natural Science

537 Foundation of China (22376031, 21925601, 92143301).

538

References

Alage, S., Michoud, V., Harb, S., Picquet-Varrault, B., Cirtog, M., Kumar, A., Rissanen, M., and Cantrell, C.: A nitrate ion chemical-ionization atmospheric-pressure-interface time-of-flight mass spectrometer (NO3- ToFCIMS) sensitivity study, Atmos. Meas. Tech., 17, 4709–4724, https://doi.org/10.5194/amt-17-4709-2024, 2024.

Berndt, T., Scholz, W., Mentler, B., Fischer, L., Herrmann, H., Kulmala, M., and Hansel, A.: Accretion Product Formation from Self- and Cross-Reactions of RO2 Radicals in the Atmosphere., Angewandte Chemie Int Ed Engl, 57, 3820–3824, https://doi.org/10.1002/anie.201710989, 2017.

Bhattacharyya, N., Modi, M., Jahn, L. G., and Ruiz, L. H.: Different chlorine and hydroxyl radical environments impact m -xylene oxidation products, Environ. Sci.: Atmos., https://doi.org/10.1039/d3ea00024a, 2023.

Bianchi, F., Kurtén, T., Riva, M., Mohr, C., Rissanen, M. P., Roldin, P., Berndt, T., Crounse, J. D., Wennberg, P. O., Mentel, T. F., Wildt, J., Junninen, H., Jokinen, T., Kulmala, M., Worsnop, D. R., Thornton, J. A., Donahue, N., Kjaergaard, H. G., and Ehn, M.: Highly Oxygenated Organic Molecules (HOM) from Gas-Phase Autoxidation Involving Peroxy Radicals: A Key Contributor to Atmospheric Aerosol, Chem Rev, 119, 3472–3509, https://doi.org/10.1021/acs.chemrev.8b00395, 2019.

Breton, M. L., Hallquist, Å. M., Pathak, R. K., Simpson, D., Wang, Y., Johansson, J., Zheng, J., Yang, Y., Shang, D., Wang, H., Liu, Q., Chan, C., Wang, T., Bannan, T. J., Priestley, M., Percival, C. J., Shallcross, D. E., Lu, K., Guo, S., Hu, M., and Hallquist, M.: Chlorine oxidation of VOCs at a semi-rural site in Beijing: significant chlorine liberation from ClNO2 and subsequent gas- and particle-phase Cl–VOC production, Atmos Chem Phys, 18, 13013–13030, https://doi.org/10.5194/acp-18-13013-2018, 2018.

Cai, X., Ziemba, L. D., and Griffin, R. J.: Secondary aerosol formation from the oxidation of toluene by chlorine atoms, Atmos Environ, 42, 7348–7359, https://doi.org/10.1016/j.atmosenv.2008.07.014, 2008.

Chang, C.-T., Liu, T.-H., and Jeng, F.-T.: Atmospheric concentrations of the Cl atom, CIO radical, and HO radical in the coastal marine boundary layer, Environ. Res., 94, 67–74, https://doi.org/10.1016/j.envres.2003.07.008, 2004.

Chen, M., Yin, M., Su, Y., Li, R., Liu, K., Wu, Z., and Weng, X.: Atmospheric heterogeneous reaction of chlorobenzene on mineral α-Fe2O3 particulates: a chamber experiment study, Front. Environ. Sci. Eng., 17, 134, https://doi.org/10.1007/s11783-023-1734-9, 2023.

572 Cubison, M. J. and Jimenez, J. L.: Statistical precision of the intensities retrieved from
573 constrained fitting of overlapping peaks in high-resolution mass spectra, Atmos. Meas. Tech.,
574 8, 2333–2345, https://doi.org/10.5194/amt-8-2333-2015, 2015.

575 DeMore, W. B., Sander, N. P., Golden, D. M., Hampson, R. F., Kurylo, M. J., Howard, C. J.,
576 Ravishankara, A. R., Kolb, C. E., and Molina, M. J.: Chemical Kinetics and Photochemical
577 Data for Use in Stratospheric Modeling, JPL Publication, 1997.

578 Ehn, M., Junninen, H., Petäjä, T., Kurtén, T., Kerminen, V.-M., Schobesberger, S., Manninen,
579 H. E., Ortega, I. K., Vehkamäki, H., Kulmala, M., and Worsnop, D. R.: Composition and
580 temporal behavior of ambient ions in the boreal forest, Atmos. Chem. Phys., 10, 8513–8530,
581 https://doi.org/10.5194/acp-10-8513-2010, 2010.

582 Ehn, M., Thornton, J. A., Kleist, E., Sipilä, M., Junninen, H., Pullinen, I., Springer, M., Rubach,
583 F., Tillmann, R., Lee, B., Lopez-Hilfiker, F., Andres, S., Acir, I.-H., Rissanen, M., Jokinen, T.,
584 Schobesberger, S., Kangasluoma, J., Kontkanen, J., Nieminen, T., Kurtén, T., Nielsen, L. B.,
585 Jørgensen, S., Kjaergaard, H. G., Canagaratna, M., Maso, M. D., Berndt, T., Petäjä, T., Wahner,
586 A., Kerminen, V.-M., Kulmala, M., Worsnop, D. R., Wildt, J., and Mentel, T. F.: A large source
587 of low-volatility secondary organic aerosol, Nature, 506, 476–479,
588 https://doi.org/10.1038/nature13032, 2014.

589 Eisele, F. L. and Tanner, D. J.: Measurement of the gas phase concentration of H2SO4 and
590 methane sulfonic acid and estimates of H2SO4 production and loss in the atmosphere, J
591 Geophys Res Atmospheres, 98, 9001–9010, https://doi.org/10.1029/93jd00031, 1993.

592 Europe, U. N. E. C. for: Globally Harmonized System of Classification and Labelling of
593 Chemicals (GHS), Glob. Harmon. Syst. Classif. Label. Chem. (GHS),
594 https://doi.org/10.18356/9789210019071, 2023.

595 Finlayson-Pitts, B. J., Keoshian, C. J., Buehler, B., and Ezell, A. A.: Kinetics of reaction of
596 chlorine atoms with some biogenic organics, Int J Chem Kinet, 31, 491–499,
597 https://doi.org/10.1002/(sici)1097-4601(1999)31:7<491::aid-kin4>3.0.co;2-e, 1999.

598 Heinritzi, M., Simon, M., Steiner, G., Wagner, A. C., Kürten, A., Hansel, A., and Curtius, J.:
599 Characterization of the mass-dependent transmission efficiency of a CIMS, Atmos Meas Tech,
600 9, 1449–1460, https://doi.org/10.5194/amt-9-1449-2016, 2016.

601 Henschler, D.: Toxicity of Chlorinated Organic Compounds: Effects of the Introduction of
602 Chlorine in Organic Molecules, Angewandte Chemie Int Ed Engl, 33, 1920–1935,
603 https://doi.org/10.1002/anie.199419201, 1994.

604 Huang, M., Wang, Z., Hao, L., and Zhang, W.: DFT study on the abstraction and addition of
605 Cl atom with toluene, Comput. Theor. Chem., 996, 44–50,
606 https://doi.org/10.1016/j.comptc.2012.07.011, 2012.

607 Huang, Y., Zhao, R., Charan, S. M., Kenseth, C. M., Zhang, X., and Seinfeld, J. H.: Unified
608 Theory of Vapor–Wall Mass Transport in Teflon-Walled Environmental Chambers, Environ.
609 Sci. Technol., 52, 2134–2142, https://doi.org/10.1021/acs.est.7b05575, 2018.

610 Jahn, L. G., McPherson, K. N., and Ruiz, L. H.: Effects of Relative Humidity and Photoaging
611 on the Formation, Composition, and Aging of Ethylbenzene SOA: Insights from Chamber
612 Experiments on Chlorine Radical-Initiated Oxidation of Ethylbenzene, ACS Earth Space
613 Chem., 8, 675–688, https://doi.org/10.1021/acsearthspacechem.3c00279, 2024.

614 Keene, William. C., Khalil, M. A. K., Erickson, David. J., McCulloch, A., Graedel, T. E.,
615 Lobert, J. M., Aucott, M. L., Gong, S. L., Harper, D. B., Kleiman, G., Midgley, P., Moore, R.
616 M., Seuzaret, C., Sturges, W. T., Benkovitz, C. M., Koropalov, V., Barrie, L. A., and Li, Y. F.:
617 Composite global emissions of reactive chlorine from anthropogenic and natural sources:
618 Reactive Chlorine Emissions Inventory, J. Geophys. Res.: Atmos., 104, 8429–8440,
619 https://doi.org/10.1029/1998jd100084, 1999.

620 Knipping, E. M., Lakin, M. J., Foster, K. L., Jungwirth, P., Tobias, D. J., Gerber, R. B., Dabdub,
621 D., and Finlayson-Pitts, B. J.: Experiments and Simulations of Ion-Enhanced Interfacial
622 Chemistry on Aqueous NaCl Aerosols, Science, 288, 301–306,
623 https://doi.org/10.1126/science.288.5464.301, 2000.

624 Krechmer, J., Lopez-Hilfiker, F., Koss, A., Hutterli, M., Stoermer, C., Deming, B., Kimmel, J.,
625 Warneke, C., Holzinger, R., Jayne, J., Worsnop, D., Fuhrer, K., Gonin, M., and Gouw, J. de:
626 Evaluation of a New Reagent-Ion Source and Focusing Ion–Molecule Reactor for Use in
627 Proton-Transfer-Reaction Mass Spectrometry, Anal Chem, 90, 12011–12018,
628 https://doi.org/10.1021/acs.analchem.8b02641, 2018.

629 Kulmala, M., Kontkanen, J., Junninen, H., Lehtipalo, K., Manninen, H. E., Nieminen, T., Petäjä,
630 T., Sipilä, M., Schobesberger, S., Rantala, P., Franchin, A., Jokinen, T., Järvinen, E., Äijälä,
631 M., Kangasluoma, J., Hakala, J., Aalto, P. P., Paasonen, P., Mikkilä, J., Vanhanen, J., Aalto, J.,
632 Hakola, H., Makkonen, U., Ruuskanen, T., Mauldin, R. L., Duplissy, J., Vehkamäki, H., Bäck,
633 J., Kortelainen, A., Riipinen, I., Kurtén, T., Johnston, M. V., Smith, J. N., Ehn, M., Mentel, T.
634 F., Lehtinen, K. E. J., Laaksonen, A., Kerminen, V.-M., and Worsnop, D. R.: Direct
635 Observations of Atmospheric Aerosol Nucleation, Science, 339, 943–946,
636 https://doi.org/10.1126/science.1227385, 2013.

637 Kürten, A., Rondo, L., Ehrhart, S., and Curtius, J.: Performance of a corona ion source for
638 measurement of sulfuric acid by chemical ionization mass spectrometry, Atmos Meas Tech, 4,
639 437–443, https://doi.org/10.5194/amt-4-437-2011, 2011.

640   Kürten, A., Rondo, L., Ehrhart, S., and Curtius, J.: Calibration of a Chemical Ionization Mass
641   Spectrometer for the Measurement of Gaseous Sulfuric Acid, J Phys Chem, 116, 6375–6386,
642   https://doi.org/10.1021/jp212123n, 2012.

643   Kürten, A., Bergen, A., Heinritzi, M., Leiminger, M., Lorenz, V., Piel, F., Simon, M., Sitals,
644   R., Wagner, A. C., and Curtius, J.: Observation of new particle formation and measurement of
645   sulfuric acid, ammonia, amines and highly oxidized organic molecules at a rural site in central
646   Germany, Atmos Chem Phys, 16, 12793–12813, https://doi.org/10.5194/acp-16-12793-2016,
647   2016.

648   Liu, X., Qu, H., Huey, L. G., Wang, Y., Sjostedt, S., Zeng, L., Lu, K., Wu, Y., Hu, M., Shao,
649   M., Zhu, T., and Zhang, Y.: High Levels of Daytime Molecular Chlorine and Nitryl Chloride
650   at a Rural Site on the North China Plain, Environ Sci Technol, 51, 9588–9595,
651   https://doi.org/10.1021/acs.est.7b03039, 2017.

652   Lu, Y., Liu, L., Ning, A., Yang, G., Liu, Y., Kurtén, T., Vehkamäki, H., Zhang, X., and Wang,
653   L.: Atmospheric Sulfuric Acid-Dimethylamine Nucleation Enhanced by Trifluoroacetic Acid,
654   Geophys Res Lett, 47, https://doi.org/10.1029/2019gl085627, 2020.

655   Ma, W., Chen, X., Xia, M., Liu, Y., Wang, Y., Zhang, Y., Zheng, F., Zhan, J., Hua, C., Wang,
656   Z., Wang, W., Fu, P., Kulmala, M., and Liu, Y.: Reactive Chlorine Species Advancing the
657   Atmospheric Oxidation Capacities of Inland Urban Environments, Environ. Sci. Technol., 57,
658   14638–14647, https://doi.org/10.1021/acs.est.3c05169, 2023.

659   Molteni, U., Bianchi, F., Klein, F., Haddad, I. E., Frege, C., Rossi, M. J., Dommen, J., and
660   Baltensperger, U.: Formation of highly oxygenated organic molecules from aromatic
661   compounds, Atmos Chem Phys, 18, 1909–1921, https://doi.org/10.5194/acp-18-1909-2018,
662   2018.

663   Orlando, J. J., Tyndall, G. S., Apel, E. C., Riemer, D. D., and Paulson, S. E.: Rate coefficients
664   and mechanisms of the reaction of cl-atoms with a series of unsaturated hydrocarbons under
665   atmospheric conditions, Int. J. Chem. Kinet., 35, 334–353, https://doi.org/10.1002/kin.10135,
666   2003.

667   Peng, X., Wang, W., Xia, M., Chen, H., Ravishankara, A. R., Li, Q., Saiz-Lopez, A., Liu, P.,
668   Zhang, F., Zhang, C., Xue, L., Wang, X., George, C., Wang, J., Mu, Y., Chen, J., and Wang,
669   T.: An unexpected large continental source of reactive bromine and chlorine with significant
670   impact on wintertime air quality, Natl. Sci. Rev., 8, nwaa304,
671   https://doi.org/10.1093/nsr/nwaa304, 2020.

672   Peng, X., Wang, T., Wang, W., Ravishankara, A. R., George, C., Xia, M., Cai, M., Li, Q.,
673   Salvador, C. M., Lau, C., Lyu, X., Poon, C. N., Mellouki, A., Mu, Y., Hallquist, M., Saiz-Lopez,
674   A., Guo, H., Herrmann, H., Yu, C., Dai, J., Wang, Y., Wang, X., Yu, A., Leung, K., Lee, S.,

and Chen, J.: Photodissociation of particulate nitrate as a source of daytime tropospheric Cl2, Nat Commun, 13, 939, https://doi.org/10.1038/s41467-022-28383-9, 2022.

Priestley, M., Breton, M. le, Bannan, T. J., Worrall, S. D., Bacak, A., Smedley, A. R. D., Reyes-Villegas, E., Mehra, A., Allan, J., Webb, A. R., Shallcross, D. E., Coe, H., and Percival, C. J.: Observations of organic and inorganic chlorinated compounds and their contribution to chlorine radical concentrations in an urban environment in northern Europe during the wintertime, Atmos Chem Phys, 18, 13481–13493, https://doi.org/10.5194/acp-18-13481-2018, 2018.

Ragains, M. L. and Finlayson-Pitts, B. J.: Kinetics and Mechanism of the Reaction of Cl Atoms with 2-Methyl-1,3-butadiene (Isoprene) at 298 K, J. Phys. Chem. A, 101, 1509–1517, https://doi.org/10.1021/jp962786m, 1997.

Riva, M., Healy, R. M., Flaud, P.-M., Perraudin, E., Wenger, J. C., and Villenave, E.: Gas- and Particle-Phase Products from the Chlorine-Initiated Oxidation of Polycyclic Aromatic Hydrocarbons., J Phys Chem, 119, 11170–81, https://doi.org/10.1021/acs.jpca.5b04610, 2015.

Shang, D., Peng, J., Guo, S., Wu, Z., and Hu, M.: Secondary aerosol formation in winter haze over the Beijing-Tianjin-Hebei Region, China, Front. Environ. Sci. Eng., 15, 34, https://doi.org/10.1007/s11783-020-1326-x, 2021.

Shi, J. and Bernhard, M. J.: Kinetic studies of Cl-atom reactions with selected aromatic compounds using the photochemical reactor-FTIR spectroscopy technique, Int. J. Chem. Kinet., 29, 349–358, https://doi.org/10.1002/(sici)1097-4601(1997)29:5<349::aid-kin5>3.0.co;2-u, 1997.

Sokolov, O., Hurley, M. D., Wallington, T. J., Kaiser, E. W., Platz, J., Nielsen, O. J., Berho, F., Rayez, M.-T., and Lesclaux, R.: Kinetics and Mechanism of the Gas-Phase Reaction of Cl Atoms with Benzene, J. Phys. Chem. A, 102, 10671–10681, https://doi.org/10.1021/jp9828080, 1998.

Tham, Y. J., Wang, Z., Li, Q., Yun, H., Wang, W., Wang, X., Xue, L., Lu, K., Ma, N., Bohn, B., Li, X., Kecorius, S., Größ, J., Shao, M., Wiedensohler, A., Zhang, Y., and Wang, T.: Significant concentrations of nitryl chloride sustained in the morning: investigations of the causes and impacts on ozone production in a polluted region of northern China, Atmos Chem Phys, 16, 14959–14977, https://doi.org/10.5194/acp-16-14959-2016, 2016.

Thornton, J. A., Kercher, J. P., Riedel, T. P., Wagner, N. L., Cozic, J., Holloway, J. S., Dubé, W. P., Wolfe, G. M., Quinn, P. K., Middlebrook, A. M., Alexander, B., and Brown, S. S.: A large atomic chlorine source inferred from mid-continental reactive nitrogen chemistry, Nature, 464, 271–274, https://doi.org/10.1038/nature08905, 2010.

708   UN: Globally Harmonized System of Classification and Labelling of Chemicals (GHS), Glob.
709   Harmon. Syst. Classif. Label. Chem. (GHS), https://doi.org/10.18356/9789210019071, 2023.

710   Vereecken, L. and Nozière, B.: H migration in peroxy radicals under atmospheric conditions,
711   Atmos. Chem. Phys., 20, 7429–7458, https://doi.org/10.5194/acp-20-7429-2020, 2020.

712   Wang, C., Collins, D. B., and Abbatt, J. P. D.: Indoor Illumination of Terpenes and Bleach
713   Emissions Leads to Particle Formation and Growth, Environ. Sci. Technol., 53, 11792–11800,
714   https://doi.org/10.1021/acs.est.9b04261, 2019.

715   Wang, C., Liggio, J., Wentzell, J. J. B., Jorga, S., Folkerson, A., and Abbatt, J. P. D.:
716   Chloramines as an important photochemical source of chlorine atoms in the urban atmosphere,
717   Proc. Natl. Acad. Sci., 120, e2220889120, https://doi.org/10.1073/pnas.2220889120, 2023.

718   Wang, D. S. and Ruiz, L. H.: Secondary organic aerosol from chlorine-initiated oxidation of
719   isoprene, Atmos Chem Phys, 17, 13491–13508, https://doi.org/10.5194/acp-17-13491-2017,
720   2017.

721   Wang, D. S., Masoud, C. G., Modi, M., and Ruiz, L. H.: Isoprene-Chlorine Oxidation in the
722   Presence of NOx and Implications for Urban Atmospheric Chemistry., Environ Sci Technol,
723   https://doi.org/10.1021/acs.est.1c07048, 2022.

724   Wang, L., Arey, J., and Atkinson, R.: Reactions of Chlorine Atoms with a Series of Aromatic
725   Hydrocarbons, Environ Sci Technol, 39, 5302–5310, https://doi.org/10.1021/es0479437, 2005.

726   Wang, M., Yang, L., Liu, X., Wang, Z., Liu, G., and Zheng, M.: Hexachlorobutadiene
727   emissions from typical chemical plants, Front. Environ. Sci. Eng., 15, 60,
728   https://doi.org/10.1007/s11783-020-1352-8, 2021.

729   Wang, S., Wu, R., Berndt, T., Ehn, M., and Wang, L.: Formation of Highly Oxidized Radicals
730   and Multifunctional Products from the Atmospheric Oxidation of Alkylbenzenes, Environ. Sci.
731   Technol., 51, 8442–8449, https://doi.org/10.1021/acs.est.7b02374, 2017.

732   Wang, Y., Riva, M., Xie, H., Heikkinen, L., Schallhart, S., Zha, Q., Yan, C., He, X.-C., Peräkylä,
733   O., and Ehn, M.: Formation of highly oxygenated organic molecules from chlorine-atom-
734   initiated oxidation of alpha-pinene, Atmos Chem Phys, 20, 5145–5155,
735   https://doi.org/10.5194/acp-20-5145-2020, 2020.

736   Wang, Y., Li, C., Zhang, Y., Li, Y., Yang, G., Yang, X., Wu, Y., Yao, L., Zhang, H., and Wang,
737   L.: Secondary reactions of aromatics-derived oxygenated organic molecules lead to plentiful
738   highly oxygenated organic molecules within an intraday OH exposure, Atmos. Chem. Phys.,
739   24, 7961–7981, https://doi.org/10.5194/acp-24-7961-2024, 2024.

740 Wingenter, O. W., Sive, B. C., Blake, N. J., Blake, D. R., and Rowland, F. S.: Atomic chlorine
741 concentrations derived from ethane and hydroxyl measurements over the equatorial Pacific
742 Ocean: Implication for dimethyl sulfide and bromine monoxide, J. Geophys. Res.: Atmos., 110,
743 https://doi.org/10.1029/2005jd005875, 2005.

744 Wu, Y., Huo, J., Yang, G., Wang, Y., Wang, L., Wu, S., Yao, L., Fu, Q., and Wang, L.:
745 Measurement report: Production and loss of atmospheric formaldehyde at a suburban site of
746 Shanghai in summertime, Atmos. Chem. Phys., 23, 2997–3014, https://doi.org/10.5194/acp-
747 23-2997-2023, 2023.

748 Xu, L., Møller, K. H., Crounse, J. D., Kjaergaard, H. G., and Wennberg, P. O.: New Insights
749 into the Radical Chemistry and Product Distribution in the OH-Initiated Oxidation of Benzene,
750 Environ. Sci. Technol., 54, 13467–13477, https://doi.org/10.1021/acs.est.0c04780, 2020.

751 Yang, G., Huo, J., Wang, L., Wang, Y., Wu, S., Yao, L., Fu, Q., and Wang, L.: Total OH
752 Reactivity Measurements in a Suburban Site of Shanghai, J Geophys Res Atmospheres, 127,
753 https://doi.org/10.1029/2021jd035981, 2022.

754 Yang, X., Ren, S., Wang, Y., Yang, G., Li, Y., Li, C., Wang, L., Yao, L., and Wang, L.:
755 Volatility Parametrization of Low-Volatile Components of Ambient Organic Aerosols Based
756 on Molecular Formulas, Environ. Sci. Technol., https://doi.org/10.1021/acs.est.3c02073, 2023.

757 Zhang, M., Chen, S., Yu, X., Vikesland, P., and Pruden, A.: Degradation of extracellular
758 genomic, plasmid DNA and specific antibiotic resistance genes by chlorination, Front. Environ.
759 Sci. Eng., 13, 38, https://doi.org/10.1007/s11783-019-1124-5, 2019.

760 Zhao, Y., Thornton, J. A., and Pye, H. O. T.: Quantitative constraints on autoxidation and dimer
761 formation from direct probing of monoterpene-derived peroxy radical chemistry, Proc National
762 Acad Sci, 115, 12142–12147, https://doi.org/10.1073/pnas.1812147115, 2018.

763